

*Fig. 18*  
Observation of small-scale structure in the harmonic emission from a uniformly irradiated low-Z shell. The origin of this structure is not understood at present.

#### REFERENCES

1. S. Jackel, B. Perry, and M. Lubin, *Phys. Rev. Lett.* **37**, 95 (1976).
2. J. Rizzo, S. Letzring, D. Villeneuve, M. C. Richardson, G. Gregory, R. S. Craxton, J. Delettrez, K. Lee, and R. Hutchison, *Proceedings of the Second Conference on Lasers and Electro-Optics (CLEO)*, Phoenix, AZ (1982).
3. K. Estabrook and W. L. Kruer, *Phys. Rev. Lett.* **40**, 42 (1978).
4. M. C. Richardson *et al.*, *Proceedings of the Ninth Int. Conf. Plasma Physics and Controlled Thermonuclear Fusion Research (IAEA)*, Baltimore, MD (1982) (to be published).

## 2.D Continuum X-Ray Spectra from UV- and IR-Laser-Produced Plasmas

A major reason for the interest in short-wavelength ( $\lambda \leq 0.5 \mu\text{m}$ ) laser fusion is the fact that absorption occurs primarily through inverse bremsstrahlung rather than through resonance absorption, thus avoiding one of the major sources of superthermal electrons. Because

of their long mean free path, these electrons can preheat the target core and tamper, thereby reducing the efficiency with which targets can be compressed.

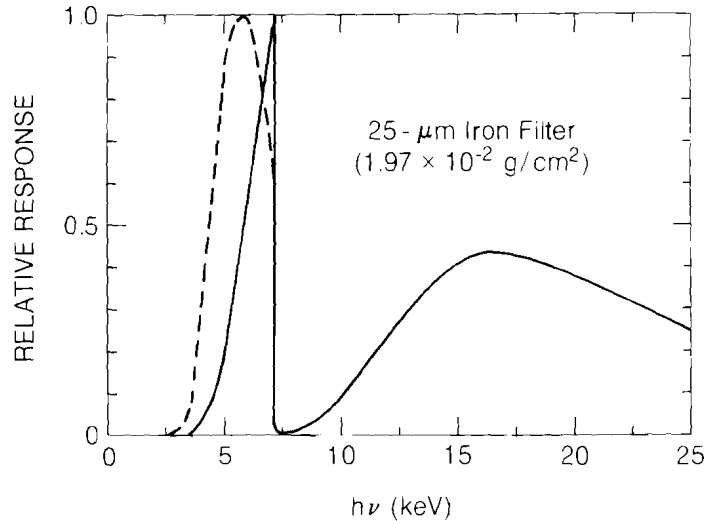
Parametric instabilities occurring in the underdense plasma may also produce fast electrons,<sup>1,2</sup> and we have previously reported observations of these instabilities in experiments conducted on the 0.35- $\mu\text{m}$  GDL facility.<sup>3</sup> In order to assess the importance of parametric instabilities as sources of fast electrons, we have measured the x-ray continuum emitted from UV-generated plasmas on GDL. The x-ray continuum, produced by electrons in the plasma as they slow down, provides a measure of the mean electron velocity (temperature) and total energy of any superthermal electron components in the plasma. We find that while there is no component attributable to resonance absorption, there is a very high temperature (20-30 keV) component which we attribute to the two-plasmon ( $2\omega_p$ ) instability. The threshold intensity for this component was found to be approximately  $2 \times 10^{14}$  W/cm<sup>2</sup>, and saturation appeared to occur above approximately  $4 \times 10^{14}$  W/cm<sup>2</sup>. The energy in this component was less than 0.1% of the incident laser energy.

### Experiment

The targets used for these experiments were planar plastic (CH) and effectively of infinite mass. The intensity on target was varied by changing both the laser energy and the focal position. Focal-spot diameters ranged from 100 to 300  $\mu\text{m}$ . The x-ray continuum was measured using K-edge-filter detectors. These detectors consist essentially of a foil absorber mounted in front of an x-ray detector. They are so named because they utilize the jump in x-ray absorption which occurs in the foil when the energy of an incident x ray is sufficient to remove an electron from the K-shell (innermost shell) of an atom in the foil. The response function for a typical K-edge filtered detector is shown in Fig. 19. While the peak response occurs in a narrow band just below the K-edge energy of the filter, there is also a broad low-level sensitivity at energies above the K-edge. If the measured x-ray spectrum is sufficiently cold, the effective response tends to be localized just below the K-edge as shown by the dashed curve in Fig. 19.

Nine silicon PIN diodes and six NaI scintillators coupled to photomultiplier tubes (PMT's) were utilized as x-ray detectors. Lead shields and collimators were incorporated in the detector arrays to ensure that only x rays produced in the target reached the detectors. The PMT detectors were calibrated using  $\text{Am}^{241}$  and  $\text{Co}^{60}$  nuclear sources; the sensitivity of silicon is well known. The signals from the detectors were integrated and recorded using gated analog-to-digital converters and a computer-controlled data-acquisition system. The signals were also monitored with oscilloscopes to check for detector saturation and to monitor the signal-to-noise ratio.

Reduction of the data from the K-edge-filter detector system is complicated by the fact that the response of the detectors is not truly narrow-band. This requires that the x-ray spectrum be obtained self-



E2408

Fig. 19  
 Response function of a typical K-edge detector (solid line). The effective response obtained with a 1-keV temperature spectrum is also shown (dashed line).

consistently over the entire range of energy covered by the full detector system. To do this we use a multi-Maxwellian model for the spectrum and assume that the spectrum can be approximated by:

$$\frac{dE}{d(h\nu)} = \sum_{j=1}^K N_j \exp(-h\nu/T_j) \quad (1)$$

In this expression,  $N_j$  and  $T_j$  are parameters which are determined through a least-squares fit to the measured data. If the electron distribution actually consists of  $K$  Maxwellians, then the parameter  $T_j$  represents the temperature of the  $j$ 'th component. Since the measurement is both time- and space-integrated and the actual electron distribution is not known, the  $T_j$  should only be loosely interpreted as representing actual electron temperatures. Our choice of spectral model is motivated by several considerations. Numerical simulations of resonance absorption<sup>4</sup> and parametric instabilities<sup>5</sup> predict electron distributions which are approximately Maxwellian. This model also permits the spectrum to be described by a small number of physically useful parameters. Finally, we find that for a suitable choice of  $K$ , we obtain good fits to the data.

We may obtain the total energy,  $E_j$ , in a superthermal electron component from the x-ray spectrum using the relation:

$$E_j = N_j / (1.6 \times 10^{10} \langle Z^2 \rangle / \langle Z \rangle) \text{ (joules)} .$$

This result, which was derived by Brueckner,<sup>6</sup> assumes that a fast electron loses its energy primarily through collisions with a cold background plasma, and neglects losses to fast ions and processes which could enhance the radiation rate. It depends only weakly on

plasma conditions and is relatively insensitive to the actual electron distribution.

### Results

A typical spectrum is shown in Fig. 20. The solid curve is obtained by using the model and procedure previously described. In order to evaluate the quality of fit and approximate range of x-ray energies measured by a particular detector, we first perform the least-squares fit and then plot the data at the locations given by:

$$\left( h\nu', \frac{S_{\text{meas}}}{S_{\text{calc}}} \frac{dE}{dh\nu} \Big|_{h\nu'} \right)$$

where  $S_{\text{meas}}$  is the measured signal and  $S_{\text{calc}}$  is the signal calculated from the best-fit spectrum  $dE/dh\nu$ . The frequency  $\nu'$  is chosen such that half of  $S_{\text{calc}}$  is produced by x rays with energy less than  $h\nu'$ . The figure illustrates a two-Maxwellian fit. We will refer to the hottest component (the segment with flattest slope) as the "superhot" component, while the other component will be referred to as cold. The component produced by resonance absorption, which is conventionally referred to as hot, is not seen in these 0.35- $\mu\text{m}$  experiments. Here we are primarily interested in the superhot component; the cold component, produced in the dense plasma near the ablation surface, will not be further mentioned.

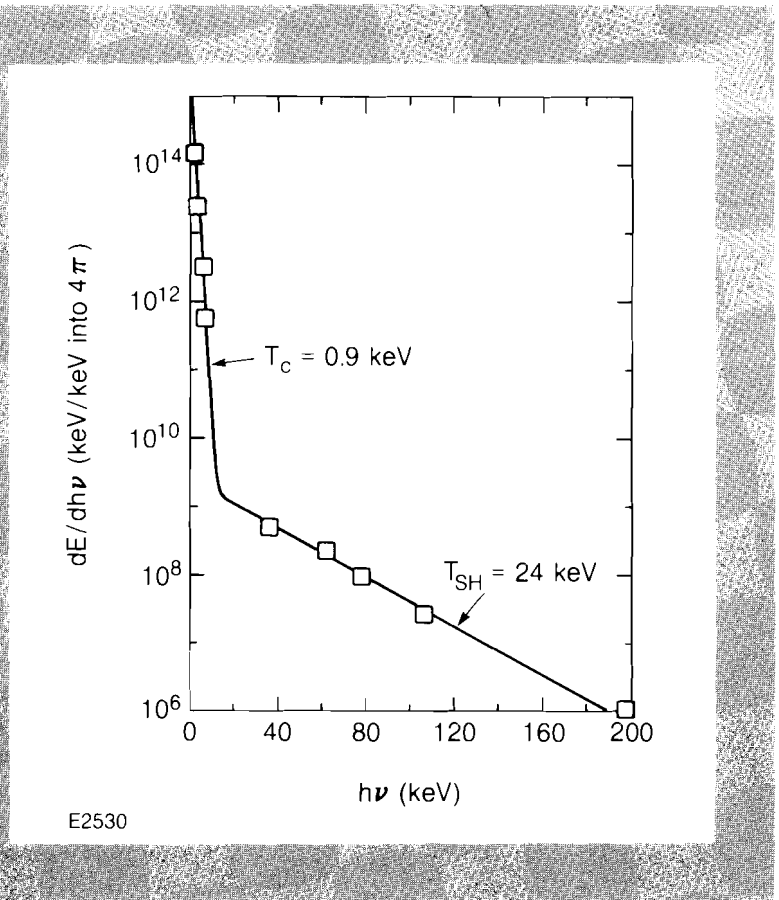


Fig. 20  
Typical two-Maxwellian spectrum obtained with 0.35- $\mu\text{m}$  irradiation. The curve is obtained using the least-squares fitting procedure outlined in the text. The data points are plotted only after the fit is obtained, and are intended to illustrate the quality of the fit and the approximate x-ray energies sampled.

Figure 21 shows the measured superhot temperature as a function of intensity. Results obtained with both 0.5-ns and 1-ns laser pulse lengths are shown. A slow  $I^{0.2}$  scaling of temperature with intensity is

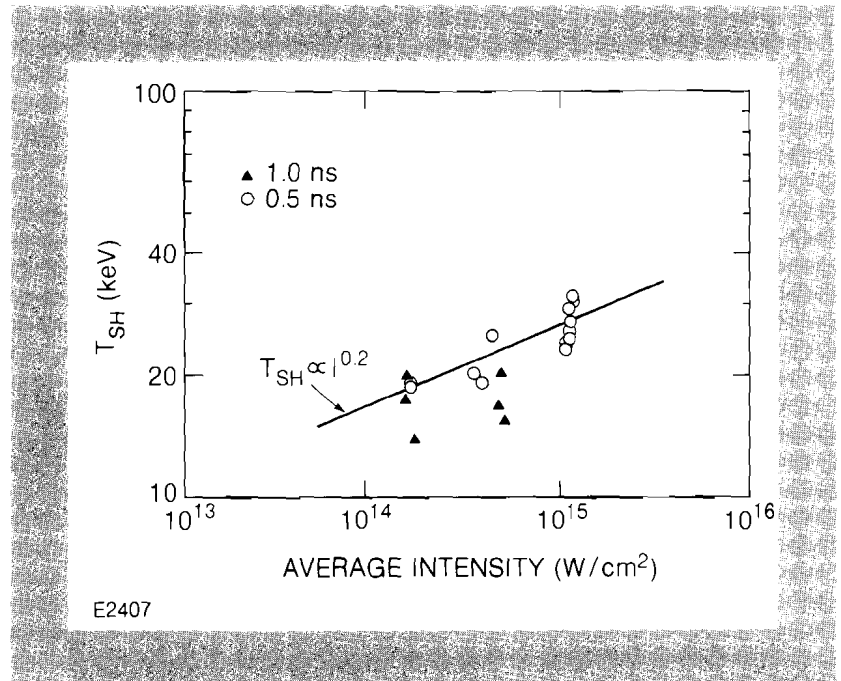


Fig. 21  
Superhot temperature as a function of incident intensity at  $0.35 \mu\text{m}$ . The solid line is a fit to the 0.5-ns data.

evident. Figure 22 shows the dependence of the superhot electron energy on the incident intensity. We note a rapid increase above approximately  $1.5 \times 10^{14} \text{ W/cm}^2$  and a subsequent saturation. This behavior is very similar to that observed for the  $\omega_0/2$  radiation emitted by these plasmas, which has been correlated with the  $2\omega_p$  instability at quarter-critical.<sup>3</sup> Because of the close correlation between the

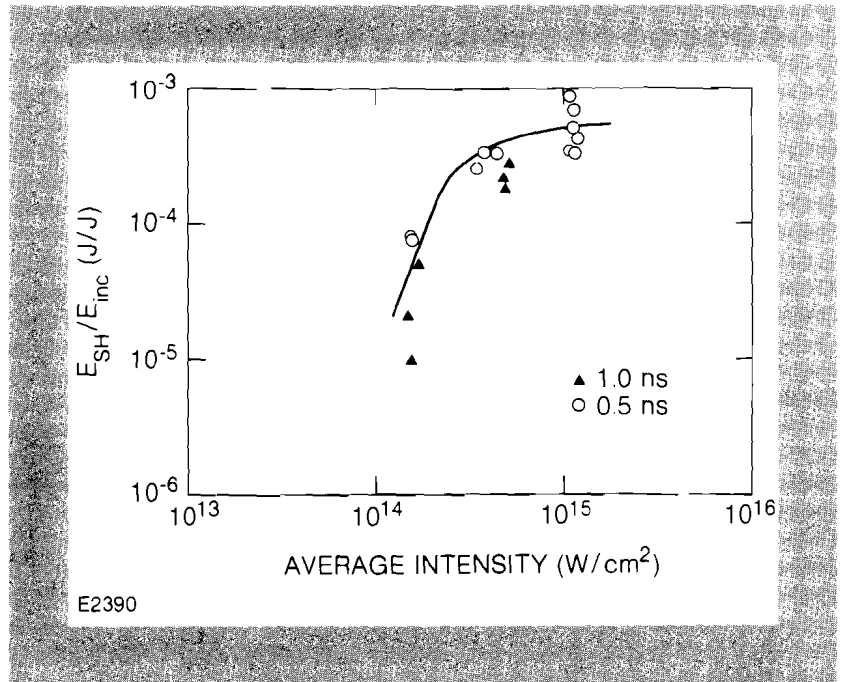


Fig. 22  
Fraction of incident energy contained in the superhot electron distribution at  $0.35 \mu\text{m}$  as inferred from the x-ray spectrum.

superhot electron energy and the  $\omega_0/2$  emission, and because no increase in the x-ray signal is observed when the Raman instability occurs, we conclude that the superhot electron distribution is produced primarily by the  $2\omega_0$  instability. The energy in the superhot distribution at saturation is small, less than 0.1% of the incident laser energy.

We performed a limited number of experiments at 1.05  $\mu\text{m}$  on the GDL system by removing the frequency-conversion crystals. This permitted us to compare the continuum spectra at the two driver wavelengths using identical instrumentation. Two spectra obtained at comparable intensities, but at the two different wavelengths, are shown in Fig. 23. We find that the superhot component is present in both cases, but the hot component produced by resonance absorption is present only at 1.05  $\mu\text{m}$ . Caution should be exercised, however, when comparing these spectra, on account of different target intensity distributions in the two cases and inadequate prepulse suppression in the IR experiments.

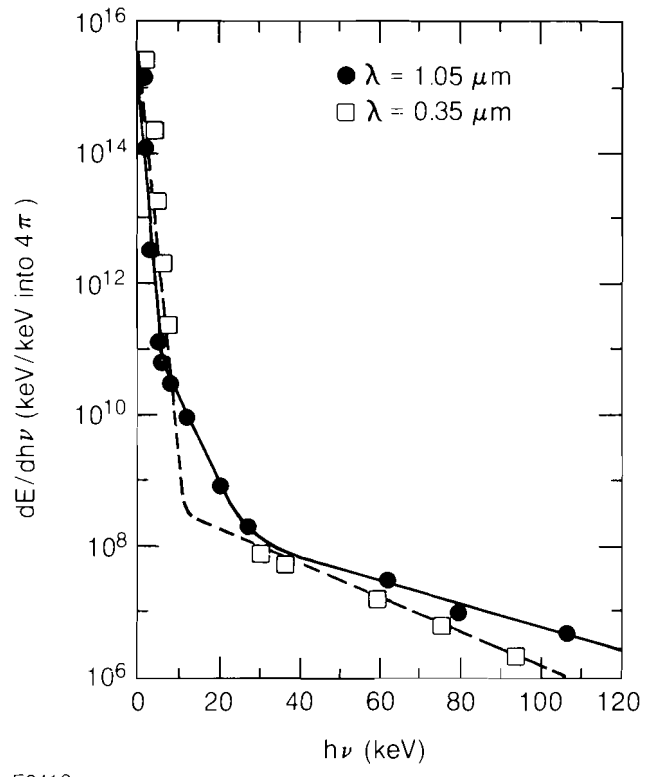


Fig. 23  
Comparison of the spectra obtained with 1.05- $\mu\text{m}$  (solid curve) and 0.35- $\mu\text{m}$  (dashed curve) incident irradiation. Both spectra were obtained on the single-beam GDL facility.

**Conclusion**

The clear absence of any x-ray signature of resonance absorption in the 0.35- $\mu\text{m}$  experiments, as well as the high measured absorptions and low preheat at 0.35  $\mu\text{m}$ ,<sup>7,8</sup> confirm that, as expected, the absorption of 0.35- $\mu\text{m}$  laser light is dominated by inverse bremsstrahlung. Thus, the most persistent and detrimental source of hot electrons in

IR-laser-produced plasmas has been removed by going to shorter wavelengths. Another interesting feature of these measurements is the presence of a superhot-electron component at both laser wavelengths. Although this component accounts for less than 0.1% of the incident laser energy in these experiments, the extent to which superhot electrons are produced in the underdense corona will have to be monitored carefully as UV-laser-generated plasmas with larger scale lengths become available.

#### REFERENCES

1. A. B. Langdon, B. F. Lasinski, and W. L. Kruer, *Phys. Rev. Lett.* **43**, 133 (1979).
2. K. Estabrook, W. L. Kruer, and B. F. Lasinski, *Phys. Rev. Lett.* **45**, 1399 (1980).
3. K. Tanaka, L. M. Goldman, W. Seka, M. C. Richardson, J. M. Soures, and E. A. Williams, *Phys. Rev. Lett.* **48**, 1179 (1982). See also LLE Review 7, (1981).
4. K. Estabrook and W. L. Kruer, *Phys. Rev. Lett.* **40**, 42 (1978).
5. B. F. Lasinski, A. B. Langdon, K. G. Estabrook, and W. L. Kruer, Lawrence Livermore 1980 Annual Report UCRL-50021-80, p. 3-30 (1981).
6. K. A. Brueckner, *Nucl. Fusion* **17**, 1257 (1977).
7. W. Seka, R. S. Craxton, J. Delettrez, R. Keck, R. L. McCrory, D. Shvarts, J. M. Soures, and R. Boni, *Opt. Commun.* **40**, 437 (1982).
8. B. Yaakobi, J. Delettrez, L. M. Goldman, R. L. McCrory, W. Seka, and J. M. Soures, *Opt. Commun.* **41**, 355 (1982).